Indian Journal of Pure & Applied Physics
Vol. 57, February 2019, pp. 132-143

Molecular structure, spectral analysis and antimicrobial activity of (E)-2-amino-8-benzylidene-4-phenyl-5,6,7,8-tetrahydro-4H-chromene-3-carbonitrile through DFT and AIM approach

Roop Kumar[a], Anil Kumar Verma[a], Huda Parveen[a], Shaheen Fatma[b], Shraddha Shukla[a], Poornima Devi[a], Nishat Afza[a] & Abha Bishnoi[a]*

[a]Department of Chemistry, Lucknow University, Lucknow 226 007, India

[b]Department of Chemistry, Shri Ramswaroop Memorial University, Lucknow, 226 001, India

Received 23 February 2018; accepted 28 August 2018

4H-pyran, (E)-2-amino-8-benzylidene-4-phenyl-5,6,7,8-tetrahydro-4H-chromene-3-carbonitrile (BCC) has been synthesised and characterized with the aid of various spectroscopic techniques, *viz.*, ^{1}H–NMR, ^{13}C-NMR, FT-IR, UV-Visible, etc. The correlation of experimental and theoretical data of structural and vibrational studies of compound has also been explored by DFT approach using B3LYP and CAM-B3LYP/6-31G (d, p) basis sets. Biological evaluation reveals that the assayed compound exhibits excellent antibacterial and antifungal activity.

Keywords: Antimicrobial activity, DFT approach, Correlation

1 Introduction

4H-pyrans are potent biologically active heterocyclic moieties and many of its derivatives manifest various biological activities such as anticancer, anticoagulant and antisplasmodic[1-3]. These 4H- pyran moieties have been often recognized as intermediates in the synthesis of many pyranopyridine, polyazanaphthalene[4], pyranopyrimidine[5] and pyridine-2-one derivatives[6]. The use of different catalysts in development of organic reactions has been an emerging area of interest for researchers in synthetic organic chemistry. L-proline has been found to be a potent catalyst in many reactions such as aldol condensation[7], synthesis of coumarins in ionic liquid[8], Mannich[9,10], Diels–Alder[11] and α-aminoxylation of aldehydes[12]. The titled compound was synthesized from (2E, 6E)-2,6-dibenzylidenecyclohexanone and malononitrile in acetonitrile under reflux conditions using L-proline as catalyst and found to be a potential antimicrobial agent[13] (Scheme 1).

The present study includes detailed analysis of optimized geometry, molecular vibrations, conformational analysis and description of electronic properties of the assayed compound. DFT approach has been employed to investigate thermodynamic properties, molecular electrostatic potential (MESP), Mulliken atomic charges, reactivity descriptors, etc. The hydrogen bonding interactions in the molecule were calculated using AIM theory.

2 Experimental Details

2.1 Materials and methods

^{1}H and ^{13}C-NMR (Nuclear Magnetic Resonance) spectra were recorded in $CDCl_3$ on Bruker 300 MHz instrument. JMS-T100LC, Accu TOF mass spectrometer gave the DART mass spectrum of the compound. FT–IR (KBr) and UV spectra (chloroform) of the molecule were recorded on a Bruker spectrometer and UV-visible Double-Beam Spectrophotometer (systronic-2203) instruments.

2.2 Synthesis of (E)-2-amino-8-benzylidene-4-phenyl-5,6,7,8-tetrahydro-4H-chromene-3-carbonitrile (BCC) and spectral record

The titled compound was synthesized from (2E, 6E)-2,6-dibenzilidinecyclohexanone (1) according to our previously reported protocol[13]. A mixture of (2E,6E)-2,6-dibenzilidinecyclohexanone **(1)** (1 mmol), malononitrile (1 mmol) and L-proline (5 mol%) in acetonitrile (10 mL) was refluxed for 5-30 min. After completion, the reaction mixture was cooled and diluted with water. The precipitate thus formed was filtered and washed with n-hexane (10 mL) to furnish the corresponding carbonitrile. Creamy fluffy solid, Yield: 89%.IR (KBr, cm^{-1}): 3428, 2359, 1648, 1560,

*Corresponding author (E-mail: abhabishnoi5@gmail.com)

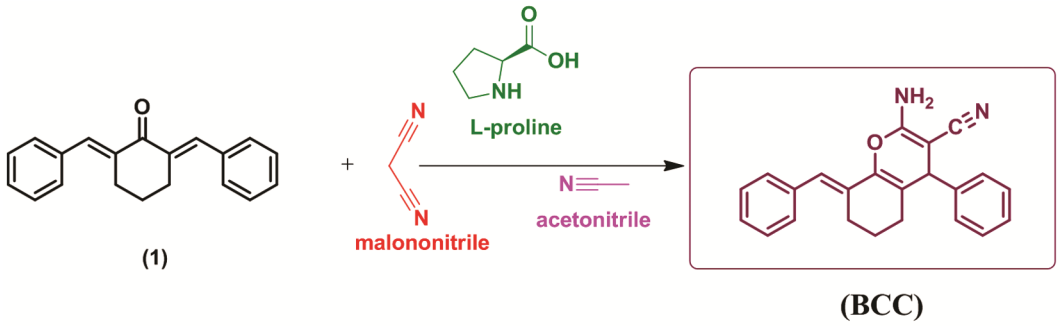

Scheme 1 – Synthetic route.

1215, 1071, 1154, 928; ^{1}H NMR (300 MHz, $CDCl_3$) δ: 1.62-1.72 (m, 2H, CH_2), 1.97-2.12 (m, 2H, CH_2), 2.54-2.76 (m, 2H, CH_2), 3.32 (s, 2H, NH_2), 3.86-4.06 (m, 1H, CH), 5.95 (s, 1H, =CH), 6.95-7.12 (m, 2H, ArH), 7.22-7.46 (m, 4H, ArH), 7.77-7.91 (m, 4H, ArH); ^{13}C NMR (75 MHz, $CDCl_3$) δ: 26.0, 30.0, 37.8, 57.7, 120.2, 127.4, 128.7, 128.8, 128.9, 129.2, 129.7, 131.9, 140.2, 145.2, 151.2, 159.1, 159.2; MS m/z: M^+ 340; Anal. Calcd for $C_{23}H_{20}N_2O$: C, 81.18; H, 5.88; N, 8.24; Found: C, 80.77; H, 5.86; N, 8.18.

The BCC was weighed and dissolved in DMSO (dimethylsulphoxide) to prepare the stock solution of 10.00 microgram/millilitre (μg/mL). The antimicrobial activity was evaluated by using Disc diffusion method by measuring the zone of inhibition in mm[20]. The antibacterial activity was compared with standard drugs. Erythromycin (E) and Vancomycin (V) were used as standard antibacterial and Fluconazole as standard antifungal drug. The minimal inhibitory concentration (MIC) was determined by micro broth dilution method using 96 well plates according to the method described by Vipra *et al.*[14]. DMSO with dilution of 1:10 was used as solvent control[14].

3 Computational Analysis

All quantum-chemical calculations were analyzed with the help of Gaussian 09 program package[15] at B3LYP and CAM-B3LYP/6-31G (d, p) basis sets. The calculated wave numbers were scaled down by using single scaling factors[16] and normal mode vibrational assignments were determined with the help of PED calculations using GAR2PED[17] program. ^{1}H NMR chemical shifts were calculated using the Gauge-Included Atomic Orbital (GIAO)[18]. The reactivity descriptors were calculated with Koopman's approximation[19,20]. The Gauss View[21] program package has been used to visualize the molecules at their optimized geometries. AIMALL program[22] has been used for AIM calculations.

4 Results and Discussion

4.1 Molecular geometry and conformational analysis

The structural parameters like bond lengths, bond angles and dihedral angles of the title compound were determined by B3LYP functional with 6-31G (d, p) basis set and are given in Table 1. The potential energy surface (PES), scans have been used for calculating the variations in the total energy of the molecule with change in dihedral angle τ(C5-C7-C11-C18) at intervals of 10° by B3LYP/6-31G (d, p) method and given in Fig. 1. The molecular structure has C1 point group symmetry. From Fig. 1 we can deduce that in the potential energy curve, three minima were observed corresponding to the conformers I, II and III with energy values of -1073.23467661, -1073.23467664 and -1073.23467660 a. u., respectively. On the basis of energy values it can be concluded that conformer II is the most stable of them all.

4.2 ^{1}H and ^{13}C NMR spectroscopy

The experimental ^{1}H and ^{13}C NMR chemical shifts together with the calculated data for the stable conformer of (BCC) are given in Table 2 which are computed by applying GIAO method using B3LYP and CAM-B3LYP/6-31G (d, p) basis sets. The experimental ^{1}H and ^{13}C NMR spectra are given in Fig. 2(a) and (b), respectively. ^{1}H NMR (300 MHz, $CDCl_3$) δ: 1.62-1.72 (m, 2H, CH_2), 1.97-2.12 (m, 2H, CH_2), 2.54-2.76 (m, 2H, CH_2), 3.32 (s, 2H, NH_2), 3.86-4.06 (m, 1H, CH), 5.95 (s, 1H, =CH), 6.95-7.12 (m, 2H, ArH), 7.22-7.46 (m, 4H, ArH), 7.77-7.91 (m, 4H, ArH); ^{13}C NMR (75 MHz, $CDCl_3$) δ: 26.0, 30.0, 37.8, 57.7, 120.2, 127.4, 128.7, 128.8, 128.9, 129.2, 129.7, 131.9, 140.2, 145.2, 151.2, 159.1, 159.2.

4.3 UV-Visible spectroscopy

A comprehensive study of UV–visible spectrum of compound (BCC) by the Time–Dependent Density Functional Theory (TD-DFT)[23] was done in order to

Table 1 – Calculated optimized geometrical parameters for compound BCC using B3LYP/6-31G (d, p) method.

Bond length (^{0}A)		Bond Angle (^{0})		Dihedral Angle (^{0})	
	B3LYP		B3LYP		B3LYP
C1-C2	1.516	C2-C1-C6	114.717	C12-C1-C2-C3	145.847
C1-C6	1.468	C1-C2-C3	111.915	C2-C1-C6-O10	-174.276
C2-C3	1.534	C3-C2-H27	110.223	C12-C1-C6-O10	6.405
C3-C4	1.529	H27-C2-H28	106.616	C6-C1-C12-H34	3.982
C2-H28	1.100	C2-C3-C29	109.888	C1-C2-C3-H29	178.513
C3-H29	1.095	C4-C5-C6	120.462	H27-C2-C3-H30	58.110
C3-H30	1.096	C1-C6-C5	125.424	C3-C4-C5-C6	21.173
C5-C7	1.516	C1-C6-O10	112.782	C4-C5-C6-O10	-179.398
C6-O10	1.399	C5-C6-O10	121.781	C1-C6-O10-C9	167.351
C9-O10	1.352	C8-C9-O10	122.924	C11-C7-C8-C9	109.943
C9-N19	1.368	C8-C9-N19	110.874	C7-C8-C9-O10	6.490
C12-C13	1.468	C6-O10-C9	119.176	C25-C8-C9-N19	6.465
C13-C20	1.409	C15-C16-C17	119.628	C8-C9-N19-H40	-151.619
C14-H35	1.087	C16-C17-C18	120.182	O10-C9-N19-H41	170.515
C16-H37	1.086	C11-C18-H39	119.507	C20-C13-C24-C23	1.689
N19-H40	1.010	C17-C18-H39	119.863	C11-C14-C15-H36	179.707
N19-H41	1.010	C9-N19-H40	115.744	C15-C16-C17-H38	179.861
C20-C21	1.391	H40-N19-H41	115.636	H42-C20-C21-C22	-179.737
C23-H45	1.086	C21-C22-C23	119.394	C21-C22-C23-C24	-0.853
C25-N26	1.168	C23-C24-H46	119.166	C22-C23-C24-H46	177.444

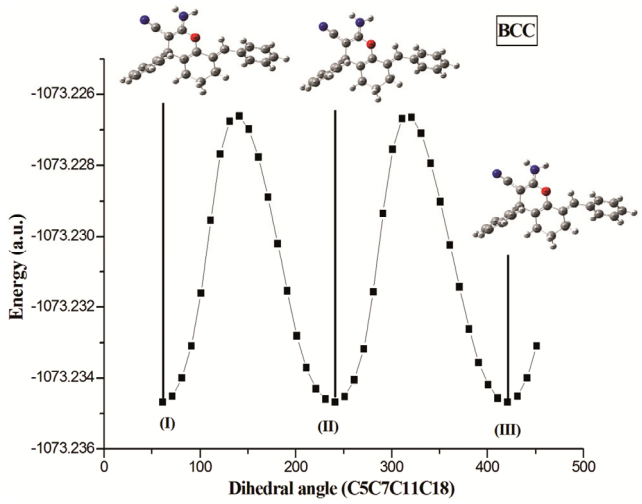

Fig. 1 – Potential energy surface scan and conformers of compound BCC.

obtain the nature of the transitions, electronic excitation energies and oscillatory strength. Comprises of electronic transitions with high oscillatory strength for molecule (BCC) and Fig. 3 contains the experimental UV-Vis spectra. The calculated electronic transitions for $\pi \rightarrow \pi^*$ and $n \rightarrow \pi^*$ at B3LYP were assigned at 307 (321) & 215 (254) nm and for CAM-B3LYP the $\pi \rightarrow \pi^*$ and $n \rightarrow \pi^*$ were assigned at 254 (254) & 277 (321) nm Table 3. The molecular orbitals of the compound and their electronic transitions revealed a clear picture of distribution of energy levels of the HOMO -7, HOMO -1 and LUMO orbitals at the B3LYP and CAM-B3LYP /6-31G (d, p) level as basis set (Fig. 4). There is an energy gap of 4.273 eV between HOMO and LUMO. As the electron-acceptor ability of electron-acceptor group is strong, hence its results in large stabilization of the LUMO and corresponding lowering of HOMO–LUMO band gap.

4.4 Vibrational spectroscopy

Figures 5 and 6 show the experimental and theoretical IR spectra of (BCC) in the region 400-4000 cm^{-1}. The scaling factor has been employed to scale down the wave numbers in order to discard an harmonicity present in real system[24]. The PED calculations have been given in Table 4 along with their theoretical (scaled) and experimental wave numbers (cm^{-1}) assignments in Table 5.

Amino and methylene groups donate electrons to aromatic ring system[25]. The N–H stretching vibration in amines is found at 3500-3300 cm^{-1}. The asymmetric and symmetric stretching vibrations of NH_2 are observed at 3450.91 and 3362.70 cm^{-1}, respectively, with 3551.89 cm^{-1} and 3437.35 cm^{-1} as their corresponding calculated values[26,27]. In benzene derivatives with NH_2 group, the scissoring mode of NH_2 is evident in the region[28,29] 1615-1650 cm^{-1}. The calculated frequency for the scissoring mode of NH_2 of the title molecule is observed at 1560.46 cm^{-1}.

Table 2 – Experimental and Calculated ^{1}H NMR and ^{13}C NMR chemical shifts of compound **BCC** using B3LYP and CAM-B3LYP/6-31G (d, p).

Atom no.	^{1}H NMR			Atom no.	^{13}C NMR		
	Calculated B3LYP	Calculated CAM-B3LYP	Experimental		Calculated B3LYP	Calculated CAM-B3LYP	Experimental
39-H	7.59	7.7313		9-C	158.61	156.8089	159.2
38-H	7.56	7.7249		11-C	144.04	127.9447	145.2
43-H	7.51	7.645		6-C	142.44	122.4885	140.2
45-H	7.45	7.5897		13-C	136.07	138.0903	131.9
36-H	7.41	7.566	7.22-7.77	1-C	130.04	113.3618	129.7
37-H	7.41	7.557		20-C	129.18	141.1351	129.2
46-H	7.39	7.4915		17-C	127.05	124.5609	128.9
44-H	7.34	7.491		14-C	126.81	125.7323	
42-H	7.31	7.4424		24-C	126.31	123.6104	128.7
35-H	7.25	7.4123		21-C	126.26	124.403	
34-H	6.97	7.0862	6.95-7.12	18-C	126.18	125.0981	
41-H	4.23	4.2849	5.95	15-C	125.80	133.9087	
33-H	3.75	4.0435	3.86-4.06	23-C	125.68	125.1177	127.4
40-H	3.67	3.7645	3.32	16-C	125.16	124.0938	
27-H	2.82	2.7133	2.54-2.56	12-C	124.85	123.244	
28-H	2.48	2.2728		22-C	124.66	124.6669	120.2
31-H	2.24	1.7663		5-C	121.38	156.8089	
32-H	1.74	1.6715	1.62-2.12				
29-H	1.49	1.5057					
30-H	1.32	1.4724					

The stretching mode of C≡N is observed at 2400 cm^{-1} and the calculated value for this mode is 2289.27 cm^{-1} in the IR spectrum[30,31]. The band at 1071.68 cm^{-1} can be the consequence of C-O stretching vibration. The calculated value for this at 989.61 cm^{-1} is in good compliance with the experimental value[32,33].

The C-C stretching vibrations[34] of the ring in aromatic hydrocarbons occur in the range of 1625-1430 cm^{-1}. There is a good agreement found between the experimental value 1648.40 cm^{-1} and calculated value 1716.08 cm^{-1} of the C=C stretching vibration in the benzene ring.

4.5 Molecular electrostatic potential

To analyse the sites of chemical reactions (electrophilicity and nucleophilicity), MEP parameters can be widely used[35-37]. The relative polarity of the molecule can also be understood pictorially with the help of MEP. Figure 7 shows the MEP of the studied compound which is obtained from optimized structure containing electropositive and electronegative regions in the molecule. Different colours at the MEP surface represent different values of the electrostatic potential; regions of maximum electrophilic reactivity, nucleophilic reactivity and zero electrostatic potential are represented by red, blue and green regions, respectively. Decrease in potential occurs as blue > green > yellow > orange > red. Major negative potential region is clearly visible around the N atom of nitrile (-CN) group as yellowish red thus accounting for the site of electrophilic attack. The rest of the molecule depicts zero electrostatic potential except for the H atom which shows positive potential.

4.6 Thermodynamic properties

All thermodynamic properties, i.e., heat capacity (CV) and entropy (*S*) are important parameters in predicting reactivity of a reaction. These parameters, (based on statistical thermodynamics and vibrational analyses), were obtained for compound BCC (Table 6). These parameters show raised values as the temperature is increased from 100 K to 500 K. Correlation between heat capacities and entropies were established with the help of quadratic formulas as shown in Fig. 8.

$$CV = 4.0442 + 0.2874T - 4.10^{-5}T^{2} \quad (R^{2} = 0.9998)$$

$$S = 71.371 + .3287T - 5.10^{-5}T^{2} \quad (R^{2} = 0.9974)$$

The change in the Gibbs free energy can be determined with the help of above equations, which in

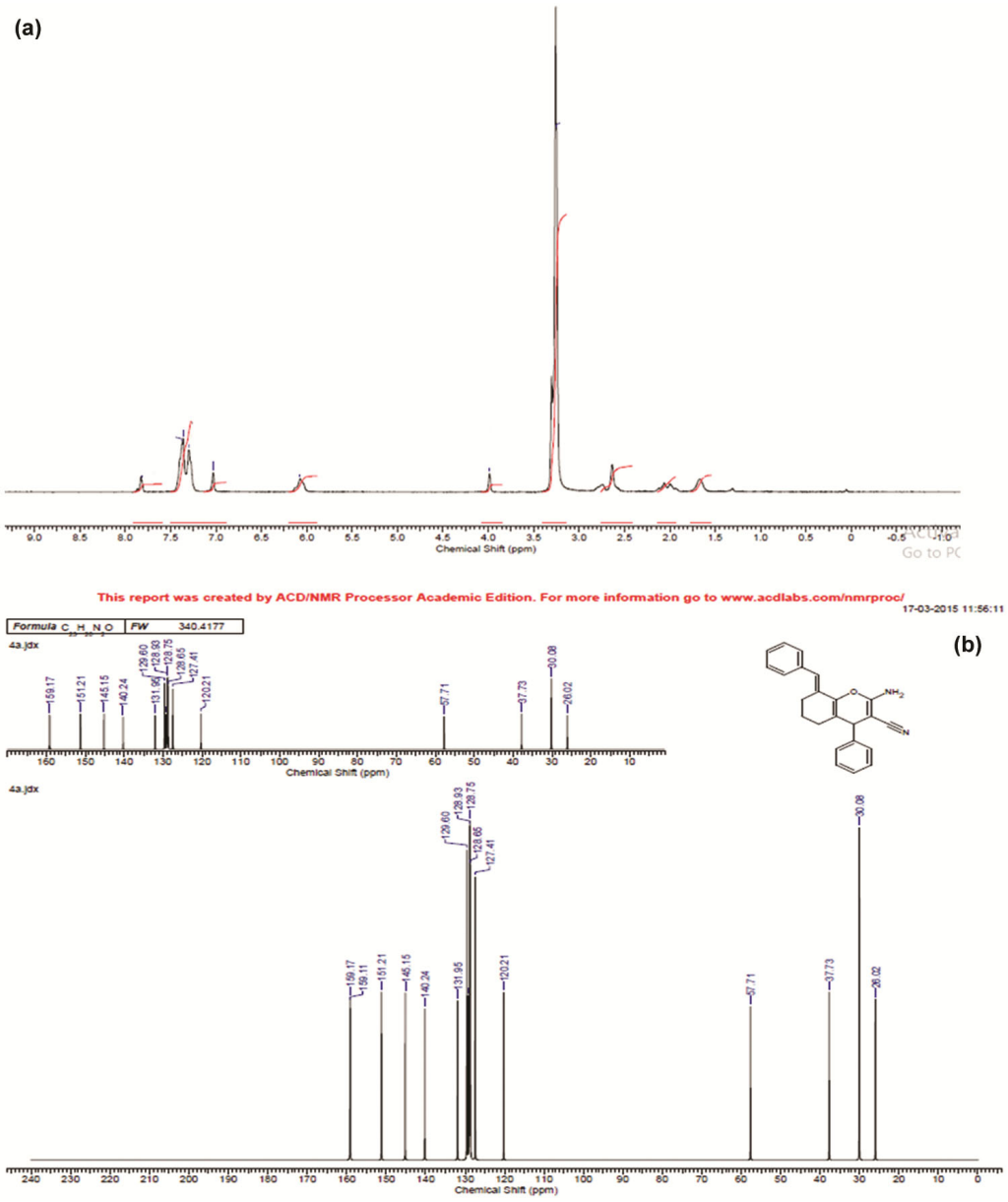

Fig. 2 – Experimental ^{1}H-NMR spectrum for compound BCC and (b) experimental^{13}C-NMR spectrum for compound BCC.

turn will give an account of spontaneity of the reaction. The thermodynamic parameters at room temperature (298.15 K) are presented in Table 7.

4.7 Chemical reactivity

4.7.1 Global and local reactivity descriptors

Significant information about energetics, structure and properties of molecules can be obtained from computational studies and were determined by density functional theoretical calculations using B3LYP and CAM-B3LYP functional with 6-31G(d,p) basis set, which are preferred over conventional ab initio wave function techniques[38].

$$\mu = \left[\frac{\partial E}{\partial N}\right]_{v(\vec{r})} = -\chi$$

$$\chi(N) = -(\partial E/\partial N)v_{(r)}$$

In accordance, the difference approximation values of chemical potential and electro negativity are given as follows:

$$\mu \approx -\frac{1}{2}(I + A) \approx \frac{1}{2}(\varepsilon_{HOMO} + \varepsilon_{LUMO})\ \chi \approx -1/2\ (\varepsilon_{HOMO} - \varepsilon_{LUMO})$$

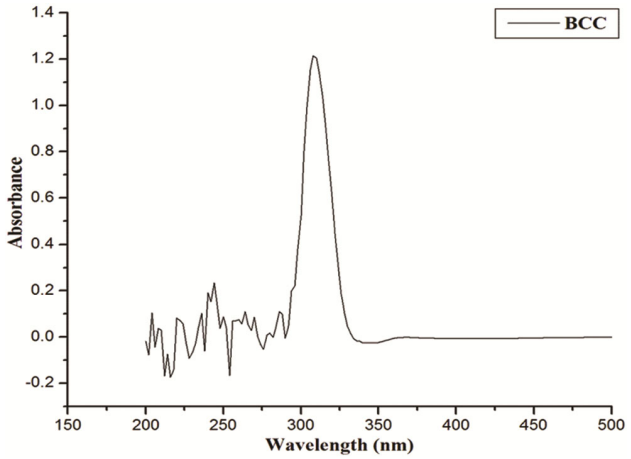

Fig. 3 – Experimental UV-Visible spectrum of the compound BCC.

Table 3 – Electronic transitions (calculated and experimental) for BCC using B3LYP and CAM- B3LYP/6-31G (d, p).

	Major contributing Molecular orbitals	*E* (eV)	Calculated (λ_{max})	Assignments	Observed (λ_{max})
B3LYP	H-1→L (63%)	4.03	307	π → π*	321
	H-7→L (61%)	5.74	215	n → π*	254
CAM-B3LYP	H→ L (40%)	4.47	277	n →π*	321
	H-1→L (45%)	4.88	254	π →π*	254

Where HOMO replaces I (ionization energy) and LUMO replaces EA (electron affinity) of the molecules as per Koopman's theorem.

The chemical hardness is represented as:

$$\eta = \frac{1}{2}\left[\frac{\partial^2 E}{\partial N^2}\right]_{v(\vec{r})} = \frac{1}{2}\left[\frac{\partial \mu}{\partial N}\right]_{v(\vec{r})} \approx \frac{1}{2}(I - A)$$

In accordance, with finite difference approximation to chemical hardness:

$$\eta \approx \frac{1}{2}(\varepsilon_{LUMO} - \varepsilon_{HOMO})$$

For insulators and semiconductors, hardness is half of the band gap.

$$S = \frac{1}{2\eta} = \left[\frac{\partial^2 N}{\partial E^2}\right]_{v(r)} = \left[\frac{\partial N}{\partial \mu}\right]_{v(r)}$$

Electrophilicity index (ω) can be calculated as under:

$$\omega = \frac{\mu^2}{2\eta}$$

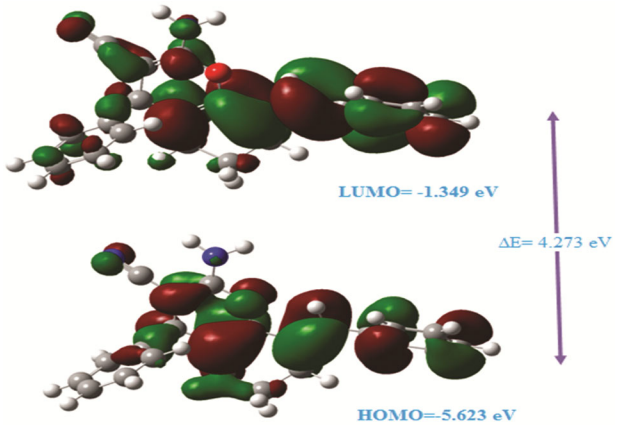

Fig. 4 – HOMO-LUMO energy gap diagram involved in electronic transitions in isolated (gaseous) phase of the compound BCC.

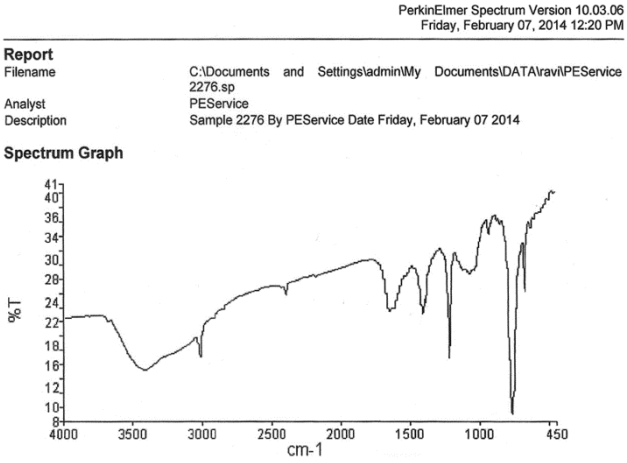

Fig. 5 – Experimental IR spectrum for compound BCC.

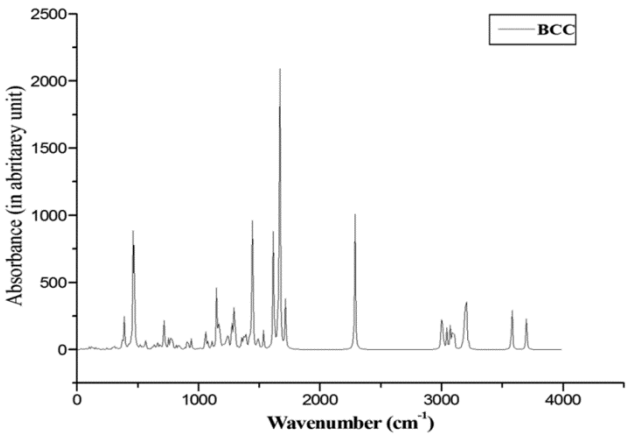

Fig. 6 – Theoretical FT-IR spectum of compound BCC.

Condensed Fukui Function is a descriptor of the reactivity of an atom in a molecule. The condensed value around each atomic site indicates the atomic contribution of molecule. The f_k values are defined as:

Table 4 – The recorded (FT-IR) and computed vibrational wavenumbers (in cm^{-1}) of **BCC** and their assignments by B3LYP/6-31G(d, p).

	Theoretical Wavenumber			
Mode	Unscaled	Scaled	Intensity(km/mol)	Vibrational Assignment (PED >10%)
51	861.21	833.56	0.06	π(H39-C11-C17-C18) (26) π(H35-C11-C15-C14) (22) π(H36-C14-C16-C15) (20) π_{asy}(H36-C14-C16-C15) (19)
52	884.33	855.94	3.11	δ (C7-C9-C8-N19) (46)
53	906.78	877.67	12.51	β(C6-C2-C1) (41) δ(C7-C9-C8-N19) (22)
54	908.94	879.76	19.91	β(C6-C2-C1) (36) δ(C7-C9-C8-N19) (20) β_{asy}(C1-C3-C2) (12)
55	927.4	897.63	1.32	υ(C5-C7) (35) υ_{asy}(C3-C4) (20) υ_{asy} (C2-C3) (16)
56	940.02	909.84	6.74	β(C1-C3-C2) (28) υ(C2-C3) (17) υ(C3-C4) (16) δ(C7-C9-C8-N19) (11)
57	941.55	911.32	18.72	β(C6-C2-C1) (23) δ(C7-C9-C8-N19) (18) β_{asy}(C1-C3-C2) (11)
58	978.38	946.97	0.04	π(H38-C16-C18-C17) (22) π_{asy}(H36-C14-C16-C15) (20) π(H39-C11-C17-C18) (17) π(H35-C11-C15-C14) (17)
59	981.51	950.00	0.52	υ(C5-C7) (20) β(C1-C3-C2) (11)
60	989.61	957.84	1.33	υ(C5-C7) (49) β_{asy}(C6-C2-C1) (15)
61	1004.45	972.20	0.32	π(H37-C15-C17-C16) (20) π_{asy}(H36-C14-C16-C15) (15) π_{asy}(H38-C16-C18-C17) (15)
62	1004.61	972.36	0.64	π(H44-C21-C23-C22) (22) π_{asy}(H45-C22-C24-C23) (20) π_{asy}(H43-C20-C22-C21) (19) τ_{asy}(C13-C20) (12)
63	1012.26	979.76	0.22	υ(C5-C7) (35) β_{asy}(C24-C20-C13) (24)
67	1057.21	1023.27	29.61	υ(C9-O10) (34) β_{asy}(C6-C2-C1) (24)
68	1072.53	1038.10	15.78	υ(C5-C7) (36) δ_{asy}(C7-C9-C8-N19) (20) υ_{asy}(C9-O10) (17) β(C6-C2-C1) (17)
69	1078.78	1044.15	6.38	υ(C5-C7) (45) υ(C2-C3) (15) δ(C7-C9-C8-N19) (13)
70	1107.85	1072.28	13.38	δ(C7-C9-C8-N19) (32) υ_{asy}(C5-C7) (24)
71	1111.34	1075.66	7.21	δ(O10-C1-C6-C2) (19) υ_{asy}(C9-O10) (15) β(C6-C2-C1) (14) υ(C5-C7) (12)
72	1148.85	1111.97	157.38	υ(C9-O10) (27) υ_{asy}(C6-O10) (24) δ(O10-C1-C6-C2) (22)
73	1167.75	1130.26	63.34	υ(C5-C7) (41) β(C6-C2-C1) (38)
74	1176.8	1139.02	26.74	υ(C5-C7) (39) β(C1-C3-C2) (21) β(C6-C2-C1) (18)
75	1181.51	1143.58	0.31	υ(C5-C7) (30) β_{asy}(C15-C37-C16) (19) β(C14-C37-C15) (11)
76	1182.79	1144.82	0.35	β (C21-H44-C22) (30) π_{asy}(H42-C13-C21-C20) (19) β_{asy}(C22-C45-C23) (17)
77	1197.60	1159.15	5.85	υ(C5-C7) (39) β(C1-C3-C2) (14)
78	1203.09	1164.47	1.59	υ(C5-C7) (18) υ(C9-O10) (14) δ_{asy}(O10-C1-C6-C2) (13)
79	1205.91	1167.20	6.17	υ(C5-C7) (52) δ_{asy}(O10-C1-C6-C2) (12)
80	1208.76	1169.95	2.65	υ(C5-C7) (44) υ(C9-O10) (19)
81	1224.4	1185.09	25.12	δ(C7-C9-C8-N19) (33) υ_{asy}(C7-C8) (27) δ_{asy}(O10-C1-C6-C2) (18)
82	1239.66	1199.86	24.18	δ(C7-C9-C8-N19) (48) υ_{asy}(C7-C8) (14)
83	1242.62	1202.73	28.37	δ(O10-C1-C6-C2) (36) β(C6-C2-C1) (24) υ(C9-O10) (13) υ(C5-C7) (12)
84	1274.63	1233.71	55.86	δ(O10-C1-C6-C2) (22) υ_{asy}(C5-C7) (21) υ(C9-O10) (18) β(C1-C3-C2) (13) δ(C7-C9-C8-N19) (13)
85	1288.86	1247.48	77.35	υ(C9-O10) (30) δ(O10-C1-C6-C2) (28) β(C1-C3-C2) (22)
86	1296.56	1254.94	78.97	δ(O10-C1-C6-C2) (25) υ(C9-O10) (24) υ_{asy}(C5-C7) (17) δ(C7-C9-C8-N19) (15)
87	1328.22	1285.58	2.61	υ(C5-C7) (53) δ(C7-C9-C8-N19) (14) υ_{asy}(C9-O10) (12)
93	1380.12	1335.81	9.64	β(C1-C3-C2) (50) υ(C3-C4) (19)
94	1391.94	1347.25	32.72	υ(C5-C7) (44) β(C1-C3-C2) (34)
95	1421.58	1375.94	39.66	δ(O10-C1-C6-C2) (43) β(C1-C3-C2) (26)
101	1501.55	1453.35	3.94	β(C1-C3-C2) (26) β(H29-H30-C3) (25) υ(C3-C4) (15) υ(C2-C3) (12)
102	1534.58	1485.32	16.16	β(C18-H38-C17) (15) β_{asy}(C11-H35-C14) (13) β_{asy}(C14-C37-C15) (13) β_{asy}(C17-H39-C18) (12)

(*Contd.*)

Table 4 – The recorded (FT-IR) and computed vibrational wavenumbers (in cm^{-1}) of **BCC** and their assignments by B3LYP/6-31G(d, p).

	Theoretical Wavenumber			
Mode	Unscaled	Scaled	Intensity(km/mol)	Vibrational Assignment (PED >10%)
103	1535.2	1485.92	25.99	δ(O10-C1-C6-C2) (16) β(C6-C2-C1) (14)
104	1616.60	1564.70	292.14	υ(C8-C9) (56) υ_{asy}(C9-O10) (26) δ(C7-C9-C8-N19) (12)
105	1622.18	1570.10	1.41	δ(O10-C1-C6-C2) (32) β(C6-C2-C1) (23) β(C6-C2-C1) (12)
106	1637.93	1585.35	0.62	υ(C5-C7) (18) δ_{asy}(C7-C9-C8-N19) (16) υ(C16-C17) (12) υ_{asy}(C15-C16) (11)
107	1650.53	1597.54	38.27	β(C6-C2-C1) (18) δ(O10-C1-C6-C2) (15)
108	1653.26	1600.19	7.9	υ(C17-C18) (19) υ(C14-C15) (18)
109	1668.7	1615.13	603.2	υ(C8-C9) (52) δ(C7-C9-C8-N19) (29)
110	1670.87	1617.23	2.55	δ(O10-C1-C6-C2) (48) β(C6-C2-C1) (29)
111	1716.08	1660.99	132.16	υ(C5-C7) (26) υ_{asy}(C5-C7) (24) β_{asy}(C6-C2-C1) (17) υ_{asy}(C8-C9) (12)
112	2289.27	2215.78	302.71	υ(C25-N26) (66) υ_{asy}(C8-N25) (10)
113	3002.97	2906.57	23.93	δ(C7-C9-C8-N19) (38) υ(C7-H33) (32)
119	3108.19	3008.41	26.09	υ(C2-H27) (46) β(C1-C3-C2) (24) β_{asy}(C6-C2-C1) (23)
120	3175.93	3073.98	11.12	υ(C14-H35) (69) υ_{asy}(C15-H36) (20)
121	3178.08	3076.06	7.18	υ(C20-H42) (62) υ_{asy}(C21-H43) (25)
122	3180.87	3078.76	3.88	υ(C18-H39) (47) υ_{asy}(C17-H38) (34)
123	3185.73	3083.46	1.99	υ(C23-H45) (43) υ_{asy}(C22-H44) (27) υ_{asy}(C12-H34) (14) υ(C20-H42) (11)
124	3188.25	3085.90	7.15	υ(C12-H34) (80)
125	3189.61	3087.22	9.85	υ(C16-H37) (41) υ_{asy}(C18-H39) υ_{asy}(C18-H39) (28) υ_{asy}(C15-H36) (17) υ_{asy}(C14-H35) (11)
126	3195.22	3092.65	46.6	υ(C21-H43) (40) υ_{asy}(C23-H45) (28) υ(C20-H42) (17) υ_{asy}(C22-H44) (12)
127	3197.14	3094.51	58.07	υ(C15-H36) (38) υ_{asy}(C17-H38) (37) υ_{asy}(C18-H39) (18)
128	3207.56	3104.59	56.77	υ(C22-H44) (51) υ(C21-H43) (30)
129	3208.29	3105.30	34.09	υ(C16-H37) (45) υ(C15-H36) (24) υ_{asy}(C17-H38) υ_{asy}(C17-H38) (23)
130	3226.88	3123.29	12.68	υ(C24-H46) (92)
131	3583.54	3468.50	116.13	υ(N19-H40) (55) υ(C19-H41) υ(N19-H41) (45)

Proposed assignment and potential energy distribution (PED) for vibrational modes: types of vibrations:
υ -symmetric stretching; υ_{asy}-asymmetric stretching; β -in-plane bending; β_{asy}-asymmetric in-plane bending;
π -symmetric out-of-plane bending; π_{asy} -asymmetric out-of-plane bending; δ -symmetric linear bend;
δ_{asy} -asymmetric linear bend; τ-torsion; τ_{asy}-asymmetric torsion.

Table 5 – Experimental FT-IR and calculated vibrational frequencies in cm^{-1} for compound BCC.

Experimental	Calculated	Vibrational Assignment
3428.61	3701.38	Asymmetric N-H stretching
3019.79	3583.54	Symmetric N-H stretching
2400	2289.27	-C≡N stretching
1648.40	1716.08	Aromatic -C=C- stretching
1560.46	1660.60	N-H in plane bending
1071.68	989.61	C-O stretching vibration

$$f_K^+ = \left[q\left(N+1\right) - q\left(N\right)\right] \text{for nucleophilic attack}$$

$$f_K^- = \left[q\left(N\right) - q\left(N-1\right)\right] \text{ for electrophilic attack}$$

$$f_K^0 = \frac{1}{2}\left[q\left(N+1\right) - q\left(N-1\right)\right] \text{ for radical attack}$$

Where, N, N-1, N+1 are total electrons present in neutral, anionic and cationic state of molecule, respectively.

The following equations define the local reactivity descriptors for site *k*:

$$s_K^+ = Sf_K^+,\ s_k^- = Sf_K^-,\ s_K^0 = Sf_K^0$$

$$\omega_K^+ = \omega f_K^+,\ \omega_K^- = \omega f_K^-,\ \omega_K^0 = \omega f_K^0$$

The maximum values indicate that the site is more liable to nucleophilic or electrophilic attack as compared to other atomic sites in reactants.

Tables 8 and 9 contain the calculated global and local reactivity parameters of BCC as derived from DFT. The high value of electrophilicity index *(ω)* = 12.988 eV for BCC than intermediate **(1)** is an indicator of its electrophilic character than dibenzylidene cyclohexanone. Therefore, the intermediate **(1)** acts as

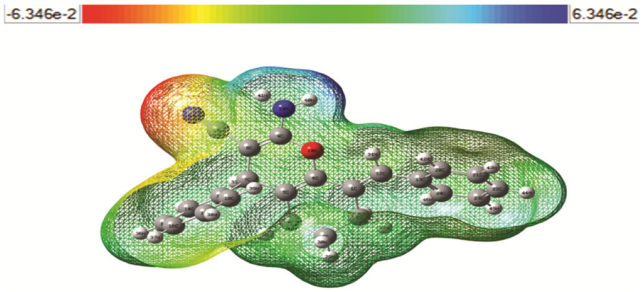

Fig. 7 – 3D plots of the molecular electrostatic potential of compound BCC.

Table 6 – Calculated thermodynamic parameters of compound BCC

Parameters	B3LYP 6-31 G (d,p)
Zero point Vibrational Energy (Kcal/mol)	235.14
Rotational Temperature (K)	0.01911
	0.00506
	0.00453
Rotational Constant (GHz)	
X	0.39819
Y	0.10537
Z	0.09446
Total Energy E_{total}(Kcal/mol)	248.91
Transational	0.889
Rotational	0.889
Vibrational	247.141

global nucleophile (electron donor) and compound BCC as a global electrophile (electron acceptor).

The maximum values of local electrophilic reactivity descriptor (f_k^+, s_k^+, ω_k^+) at N19, C22, C24, C25 indicate that these sites are liable to nucleophilic attack[39]. On the other hand, the higher values of local reactivity descriptors (f_k^-, s_k^-, ω_k^-) at C2, C9 and C12 clearly prove that these sites are more prone to electrophilic attack.

4.8 AIM calculation

The strength of hydrogen bond can be characterised by topological parameters. The interactions may be classified as per Rozas *et al.*[40] as: (i) strong H-bonds are $\nabla^2\rho_{(BCP)} < 0$ and $H_{BCP} < 0$ (ii) Medium H-bonds are $\nabla^2\rho_{(BCP)} > 0$ and $H_{BCP} < 0$ and (iii) Weak H-bonds are $\nabla^2\ \rho_{(BCP)} > 0$ and $H_{BCP} > 0$. Molecular graph of the compound BCC at B3LYP/6-31G (d, p) level using AIM program is presented in Fig. 9. Geometrical as well as topological parameters are tabulated in Table 10, and in accordance to above criteria, as $\nabla^2\ \rho_{(BCP)}$ and H_{BCP} parameters were more than zero, hence O10….H34 and H27….H46

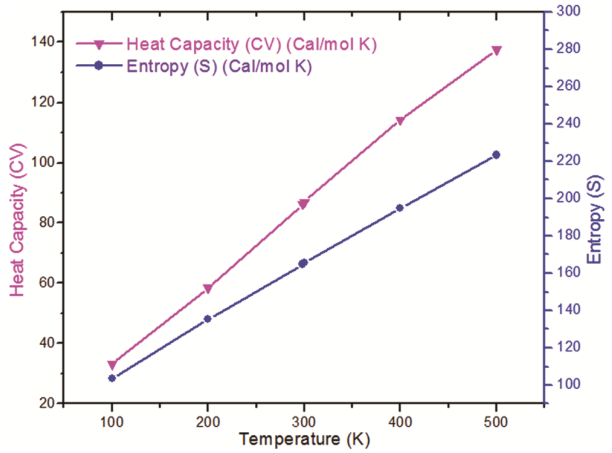

Fig. 8 – Correlation graph of thermodynamic functions at different temperatures.

Table 7 – Thermodynamic functions at different temperatures.

Temperature (T) (K)	Heat Capacity(CV) (Cal/mol K)	Entropy (S) (Cal/mol K)
100	33.129	103.593
200	58.560	135.49
298.15	86.251	164.84
300	87.043	165.39
400	114.358	194.81
500	137.60	223.36

suggesting that all the interactions are weak. The non-covalent nature of H-bond could be confirmed by the ratio $-G_{(BCP)}/V_{(BCP)}$ of the synthesized compound which was greater than unity. As per AIM calculation, the total energy of intra molecular interaction for BCC was calculated as -5.32 k cal/mol.

4.9 In vitro antibacterial activity

Antimicrobial activities were evaluated by measuring the diameter of zone of inhibition against tested organism and results are given in Table 11. The minimal inhibitory concentration values were also examined and the results are illustrated in Table 12. Antimicrobial activities of the synthesized compounds were quantitatively determined in terms of minimum inhibitory concentration values. IC_{50} is the concentration of the synthesized compounds at which 50% inhibition of test bacteria was achieved whereas MIC_{90} is the concentration of compounds at which 90% inhibition of test strain was observed. Compound BCC showed MIC value of 1.56 against *Bs*[b] MTCC 441 and *Sa*[a] MTCC 96, slightly lower than that of reference drug Erythromycin (MIC=2.49 and 1.9 µg/mL), which implies that the compound BCC might be more active than reference drug Erythromycin.

Table 8 – Calculated $\varepsilon_{HOMO,}$ ε_{LUMO}, energy band gap $\varepsilon_{LUMO} - \varepsilon_{HOMO,}$ ionization potential (IP), electron affinity (EA), electronegativity (χ), global hardness (η), chemical potential (μ), global electrophilicity index (ω), and global softness (S) in eV for intermediate **(1)** and product **(BCC)**, using B3LYP and CAM-B3LYP/6-31G(d,p).

	ϵ_H	ϵ_L	ϵ_H-ϵ_L	I	A	χ	η	μ	ω	S
Intermediate (**1**)	-6.293	-2.224	-4.069	6.293	2.224	4.258	2.034	-4.258	4.456	0.226
Product (**BCC**) B3LYP	-5.623	-1.349	-4.273	5.623	1.349	3.486	2.136	-3.486	12.988	1.068
Product (**BCC**) CAM-B3LYP	-7.009	-0.036	-6.972	7.009	0.036	3.523	3.486	-3.523	1.780	1.743

Table 9 – Using Hirshfeld populations analysis: Fukui functions (fk^+, fk^-), Local softnesses (sk^+, sk^-) in eV, local electrophilicity indices (ωk^+, ωk^-) in eV for selected atomic sites of compound BCC.

	Hirshfeld atomic charges			Fukui functions		Local softness		Local electrophilicity indices	
Atom No.	q_N	q_N+1	q_N-1	f_k^+	f_k^-	sk^+	sk^-	ωk^+	ωk^-
1C	0.025088	0.09706	0.06365	0.071972	-0.03856	0.076893	-0.0412	0.934782	-0.50085
2C	0.03184	0.022022	-0.06378	-0.00982	0.095623	-0.01049	0.102161	-0.12752	1.241965
3C	0.007682	0.055951	-0.03969	0.048269	0.047369	0.051569	0.050608	0.626925	0.615235
4C	-0.00012	0.063714	-0.06737	0.063837	0.067247	0.068202	0.071845	0.829124	0.873413
5C	0.045567	0.107134	0.004186	0.061567	0.041381	0.065776	0.04421	0.799641	0.537462
6C	0.276802	0.316318	0.257631	0.039516	0.019171	0.042218	0.020482	0.513239	0.248996
7C	-0.09166	-0.07821	-0.12737	0.013455	0.035705	0.014375	0.038146	0.174755	0.463742
8C	0.100485	0.088462	0.020325	-0.01202	0.08016	-0.01285	0.085641	-0.15616	1.041129
9C	0.63882	0.558647	0.526896	-0.08017	0.111924	-0.08565	0.119576	-1.0413	1.453685
10O	-0.58238	-0.53246	-0.55271	0.04992	-0.02968	0.053333	-0.03171	0.648368	-0.38546
11C	0.147902	0.151791	0.167118	0.003889	-0.01922	0.004155	-0.02053	0.050511	-0.24958
12C	-0.05445	-0.01149	-0.20027	0.042962	0.145817	0.045899	0.155787	0.557996	1.893892
13C	0.144271	0.114025	0.119463	-0.03025	0.024808	-0.03231	0.026504	-0.39284	0.32221
14C	-0.03637	-0.02563	-0.07922	0.010736	0.042849	0.01147	0.045779	0.139441	0.556529
15C	-0.00327	0.041609	-0.0318	0.044879	0.028527	0.047947	0.030477	0.582895	0.370513
16C	-0.00173	0.043624	-0.04584	0.045354	0.044108	0.048455	0.047124	0.589064	0.572881
17C	-0.00462	0.03352	-0.03743	0.03814	0.032812	0.040748	0.035055	0.495368	0.426167
18C	-0.0273	-0.03712	-0.02347	-0.00982	-0.00383	-0.01049	-0.0041	-0.12749	-0.04978
19N	-0.09659	-0.00638	-0.12657	0.090206	0.029982	0.096374	0.032032	1.171608	0.38941
20C	-0.05162	0.01246	-0.09671	0.064083	0.045089	0.068464	0.048172	0.832319	0.585622
21C	-0.01061	0.049766	-0.05925	0.060373	0.048638	0.064501	0.051963	0.784133	0.631717
22C	0.001255	0.07975	-0.09305	0.078495	0.0943	0.083862	0.100747	1.019504	1.224782
23C	-0.03879	0.044723	-0.06006	0.083516	0.021268	0.089226	0.022722	1.084718	0.276232
24C	-0.02683	0.010065	-0.08642	0.036898	0.059582	0.039421	0.063656	0.479236	0.773859
25C	0.134072	0.254407	0.194816	0.120335	-0.06074	0.128563	-0.0649	1.562928	-0.78895
26N	-0.52743	-0.45375	-0.5631	0.073676	0.035671	0.078713	0.03811	0.956914	0.4633

Table 10 – Topological parameters for bonds of interacting atoms: electron density (ρ_{BCP}), Laplacian of electron density ($\nabla^2\rho_{(rBCP)}$), electron kinetic energy density (G_{BCP}), electron potential energy density (V_{BCP}), total electron energy density (H_{BCP}) at bond critical point (BCP) and estimated interaction energy (E_{int}) for compound **BCC**.

Interaction	$\rho_{(BCP)}$	$\nabla^2\rho_{(rBCP)}$	G_{BCP}	V_{BCP}	H_{BCP}	E_{int}
O10 - H34	+0.0166	+0.0735	+0.0156	-0.012	0.003	-3.76
H27 - H46	+0.0102	+0.0422	+0.0079	-0.005	0.002	-1.56

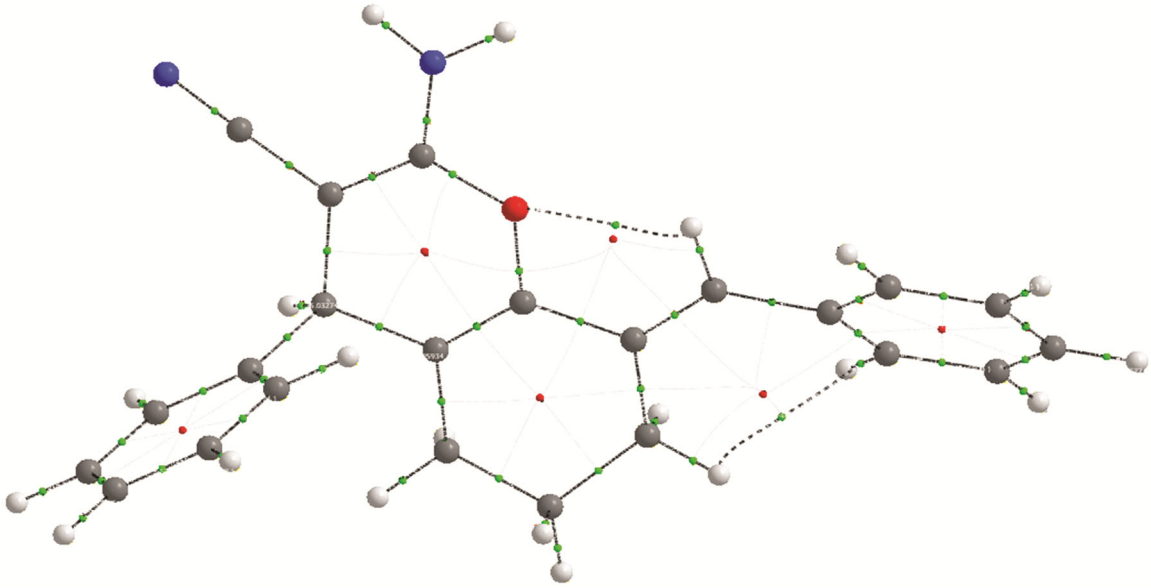

Fig. 9 – Molecular graph of compound BCC: bond critical points (small green spheres), ring critical points (small red sphere) and bond paths (grey lines).

Table 11 – Antibacterial and antifungal activities of synthesized compound **BCC** against different Strains (diameter of zone of inhibition).

Compound	Zone of inhibition (mm) of bacterial strains									Zone of inhibition (mm) of fungal strains			
	Bs[a]	*Bs*[b]	*Bp*	*Sa*[a]	*Sa*[b]	*Pv*	*St*	*Pa*	*Ec*	*Ca*	*Ct*	*An*	*Pc*
BCC	**21**[b]	16	06[a]	**19**[b]	12	06[a]	06[a]	11[a]	12	08[a]	09[a]	06[a]	06[a]

Table 12 – Antimicrobial activity of BCC (MIC (µg/mL) against different strains) using 96 well plate by micro broth dilution method.

S.No.	Bacterial Strains	MIC(µg/mL)						
		BCC		E		Fungal strains	BCC	Fluconazole
		90	**50**	**90**	**50**			
1.	*Bs*[a] MTCC121	25	9.36	3.00	2.3	*Ct*	125	12.5
2.	*Bs*[b] MTCC441	36.92	**1.56**[a]	3.67	2.49	*Ca*	125	6.25
3.	*Bp* MTCC1607	27.95	10.19	1.5	<0.39	*An*	125	-
4.	*Sa*[a] MTCC96	37	**1.56**[a]	2.75	1.9	*Pc*	125	-
5.	*Sa*[b] MTCC902	31.4	23.7	0.37	<0.39			
6.	*Pv* MTCC 426	26.74	12.5	<0.39	<0.39			
7.	*St* MTCC537	12.85	6.25	6.78	<0.39			
8.	*Pa* MTCC741	28.60	16.59	3.98	<0.39			
9.	*Ec* MTCC1304	100	50	9.62	<0.39			

[a]Entries in bold font indicate lower MIC values than reference drug Erythromycin.

5 Conclusions

The compound BCC has been well characterized with the help of ^{1}H, ^{13}C NMR, FT-IR, UV-visible spectroscopy and mass spectrometry. Conformational analysis showed the most stable conformer is II with energy values of -1073.23467660 a.u. at room temperature. The energy gap between the HOMO and LUMO confirms that BCC possess low kinetic stability and high chemical reactivity. Molecular electrostatic potential surface analysis exhibited that the nitrogen atom of nitrile (-CN) group is the binding site for electrophilic attack. The global electrophilicity index of BCC is 12.988 eV indicating that molecule may act as a good electrophile. In BCC, the weak intramolecular interactions were confirmed on the basis of AIM approach. Compound (BCC) was found to exhibit excellent activity against *B. subtilis* (*Bs*[b]) MTCC 441 and *S. aureus* (*Sa*[a]) MTCC 96. Hence, it

can be concluded that there is ample scope for further study in developing new derivatives of BCC as good lead compounds for the treatment of bacterial strains. The molecule is suitable for the generation of bioactive molecular assemblies as well as for the preparation of other heterocycles.

Acknowledgement

The authors are grateful to the Head, Department of Chemistry, University of Lucknow, Lucknow, for providing necessary laboratory facilities. The authors thank the SAIF facility of Central Drug Research Institute (CDRI), Lucknow for providing spectral, elemental and biological activity data.

References

1 Witte E C, Neubert P & Roesch A, *Chem Abst*, 104 (1986) 224915F.
2 Bonsignore L, Loy G D & Calignano A, *Eur J Med Chem*, 28 (1993) 517.
3 Abdelrazek F M, Metz P, Kataeva O, Jager A & El-Mahrouky S F, *Arch de Pharm,* 340 (2007) 543.
4 Lei M, Ma L & Hu L, *Tetrahedron Lett*, 52 (2011) 2597.
5 Adbel-Fattah A H, Hesien A M, Metwally S A & Elnagdi M H, *L Annal De Chem,* (1989) 585.
6 Qintela J M, Peinador C & Moreira M J, *Tetrahedron,* 51 (1995) 5901.
7 Alcaide B, Almendros P, Luna A & Torres M R, *J Org Chem*, 71 (2006) 4818.
8 Liu X H, Fan J C, Liu Y & Shang Z C, *J Zhejiang Univ Sci B,* 9 (2008) 990.
9 Jane J M, Hsiao Y & Armstrong J D, *J Org Chem,* 71 (2006) 390.
10 List B, Pojarliev P, Biller W T & H J Martin, *J Am Chem Soc,* 124 (2002) 827.
11 Ramachary D B, Chowdari N S & Barbas C F, *Angew Chem,* 115 (2003) 4365.
12 Wang H, Yang C & Han K, *Struct Chem,* 17 (2006) 97.
13 Verma A K, Bishnoi A, Fatma S, Srivastava A & Singh V, *D Phar Chem*, 8 (2016) 380.
14 Vipra A, Desai S N, Junjappa R P, Roy P, Poonacha N, Ravinder P, Sriram B & Padmanabhan S, *Adv Microbiol*, 3 (2013) 181.
15 Frisch M J, Trucks G W, Schlegel H B, Scuseria G E, Robb M A, Cheeseman J R, Scalmani G, Barone V, Mennucci B, Petersson G A, Nakatsuji H, Caricato M, Li X, Hratchian H P, Izmaylov A F, Bloino J, Zheng G, Sonnenberg J L, Hada M, Ehara M, Toyota K, Fukuda R, Hasegawa J, Ishida M, Nakajima T, Honda Y, Kitao O, Nakai H, Vreven T, Montgomery J A, Peralta J E, Ogliaro F, Bearpark M, Heyd J J, Brothers E, Kudin K N, Staroverov V N, Keith T, Kobayashi R, Normand J, Raghavachari K, Rendell A, Burant J C, Iyengar S S, Tomasi J, Cossi M, Rega N, Millam J M, Klene M, Knox J E, Cross J B, Bakken V, Adamo C, Jaramillo J, Gomperts R, Stratmann R E, Yazyev O, Austin A J, Cammi R, Pomelli C, Ochterski J W, Martin R L, Morokuma K, Zakrzewski V G, Voth G A, Salvador P, Dannenberg J J, Dapprich S, Daniels A D, Farkas O, Foresman J B, Ortiz J V, Cioslowski J & Fox D J, *Gaussian 09*, *Revision E01*, *Gaussian, Inc, Wallingford CT*, 2013.
16 Andersson M P & Uvdal P, *J Phys Chem,* 109 (2005) 2937.
17 Martin J M L, Alsenoy V & Alsenoy C V, 1995 Gar2ped University of Antwerp, 1995.
18 Zhengyu Z, Aiping F & Dongmei D, *J Quantum Chem*, 78 (2000) 186.
19 Chattaraj P K, Giri S, Duley S, Electrophilicity Index, *Chem Rev*, 111 (2011) PR43-PR75.
20 Klopman G, *J Am Chem Soc*, 90 (1968) 223.
21 Frisch A, Nielson A B & Holder A J, *GaussView user manuual*, Gaussian Inc, Pittsburgh, P A, 2005.
22 Keith T A, AIMAll (Version 100504, Professional), 1997-2010.
23 Jin R, Sun W & Tang S, *Int J Mol Sci*, 13 (2012) 10986.
24 Rawat P, Singh R N & Sahu S, *J Mol Struct,* 1076 (2014) 437.
25 Colthup N B, Daly L H & Wiberley S E, *Introduction to infrared and raman spectroscopy*, 3rd Edn, (Academic Press: Boston), 1990.
26 Gunasekaran S, Varadhan S R & Manoharan K, *Asian J Phys*, 2 (1993) 165.
27 Gunasekaran S, Varadhan S R & Manoharan K, *Ind J Phys*, 67B (1993) 95.
28 Yadav R A & Singh I S, *Ind J Pure Appl Phys*, 23 (1985) 626.
29 Wiberg K B & Shrake A, *Spectrochim Acta*, 29A (1973) 583.
30 Roeges N P G, *A guide to the complete interpretation of infrared spectra of organic structures*, (John Wiley and Sons Inc: New York), 1994.
31 Gnanasambanadan T, Gunasekaran S & Seshadri S, *Res J Chem Environ*, 17 (2013) 42.
32 Druzbicki K, Mikuli E & Chrusciel M D O, *Vib Spectrosc*, 52 (2010) 54.
33 Dolega D, Mikuli A M & Chrusciel J, *J Mol Struct,* 933 (2009) 30.
34 Manohar S, Nagalakshmi R & Krishnakumar V, *Spectrochim Acta Part A*, 71 (2008) 110.
35 Joshi B D, Srivastava A, Honorato S B, Tandon P, Pessao O D L, Fechine P B A & Ayala A P, *Spectrochim Acta Part A,* 113 (2013) 367.
36 Xavier R J & Dinesh P, *Spectrochim Acta Part A,* 118 (2014) 999.
37 Govindarajan M & Karabacak M, *Spectrochim Acta Part A,* 96 (2012) 421.
38 Brak K & Jacobsen E N, *Angew Chem Int Ed Engl*, 52 (2013) 534.
39 Koch U & Popelier P, *J Phys Chem A*, 99 (1995) 9747.
40 Rozas I, Alkorta I & Elguero J, *J Am Chem Soc*, 122 (2000) 11154.